# Orbit determination based on meteor observations using numerical integration of equations of motion

Vasily Dmitriev[1] *, Valery Lupovka[1], and Maria Gritsevich[1,2,3]

[1]Moscow State University of Geodesy and Cartography (MIIGAiK), Extraterrestrial Laboratory
[2] Finnish Geospatial Research Institute (FGI), Department of Geodesy and Geodynamics, Geodeetinrinne 2, P.O. Box 15, FI-02431 Masala, Finland
[3]Russian Academy of Sciences, Dorodnicyn Computing Centre, Department of Computational Physics, Vavilova 40, 119333 Moscow, Russia
*Corresponding author. E-mail: vm.dmitriev90@gmail.com

**Abstract**

Recently, there has been a worldwide proliferation of instruments and networks dedicated to observing meteors, including international airborne campaigns (Vaubaillon, J. et al., 2015) and possible future space-based monitoring systems (Bouquet A., et al., 2014). There has been a corresponding rapid rise in high quality data accumulating annually. In this paper, we present a method embodied in a software program, which can effectively and accurately process these data in an automated mode and discover the pre-impact orbit and possibly the origin or parent body of a meteoroid or asteroid. The required input parameters are the topocentric pre-atmospheric velocity vector and the coordinates of the atmospheric entry point of the meteoroid, i.e. the beginning point of visual path of a meteor, in the an Earth centered-Earth fixed coordinate system, the International Terrestrial Reference Frame (ITRF). Our method is based on strict coordinate transformation from the ITRF to an inertial reference frame and on numerical integration of the equations of motion for a perturbed two-body problem. Basic accelerations perturbing a meteoroid's orbit and their influence on the orbital elements are also studied and demonstrated. Our method is then compared with several published studies that utilized variations of a traditional analytical technique, the zenith attraction method, which corrects for the direction of the meteor's trajectory and its apparent velocity due to Earth's gravity. We then demonstrate the proposed technique on new observational data obtained from the Finnish Fireball Network (FFN) as well as on simulated data. In addition, we propose a method of analysis of error propagation, based on general rule of covariance transformation.

**Introduction**

Improving existing techniques, derived from ground based observations, and developing new methods that more accurately determine meteor orbits are among the goals of meteor astronomy.

Typically, an analysis of meteor observations yields the azimuth and the inclination of the atmospheric trajectory (i.e. a topocentric radiant) of a meteor, its apparent velocity, and the

coordinates of the origin of its visual path. These data are sufficient to determine the pre-impact heliocentric orbit of the meteoroid. Knowing the heliocentric orbit may lead to discovery of the meteoroid's parent body or its origin. In the past several authors conducted an analysis of the dynamical evolution of asteroid or meteoroid's orbits. To implement this, they employed a numerical integration of equations of motions over a long time backwards from the impact date. For example, in the works (de la Fuente Marcos & de la Fuente Marcos, 2013, Trigo-Rodriguez, et al., 2015) a backward integration was performed for period of at least 10000 years. If there are sufficient uncertainties in the initial conditions, then they can negate the value of this type of analysis.

It is obvious, that the greatest changes to an asteroid`s or meteoroid`s orbit occur just prior to its encounter with Earth. Thus, in determining the orbit we have to be very precise and careful when we consider the influences of all the corrections and perturbing forces. As a meteoroid approaches Earth, its orbit changes, primarily under the influence of Earth's gravity. Currently, a "zenith attraction" technique is widely used to account for this effect. The zenith attraction method employs corrections to compensate for Earth's gravity effect on the direction of the meteor's trajectory and its apparent velocity.

This technique was described and used to determine the orbits of meteors registered by the cameras of European Fireball Network in (Ceplecha, 1987). Implementations of the zenith attraction method have also been published in several software packages, for example, in (Zoladek, 2011) and in (Langbroek, 2004). In recent analysis by (Clark & Wiegert, 2011) and (Zuluaga, Ferrin, & Geens, 2013) a backward numerical integration was performed in place of the traditional calculation of zenith attraction corrections. The authors took into account the perturbations from Earth and other planets as point masses.

In addition to the influence of Earth, as a point mass, a meteoroid's orbit is also influenced by the attraction of the Moon, atmospheric drag, the non-central part of the Earth's gravity, and by the attraction of other solar system planets. In the past some of these effects could be neglected due to the low accuracy determination of the apparent track of a meteor. However, the recent, more precise, data collected by the dedicated fireball networks (which are well established in Central Europe, USA, Canada, Finland, Spain, Australia and other countries), do allow for an accurate determination of a meteor's trajectory. The orbital parameters of several meteorite producing fireballs, as detected by the instruments of these fireball networks, were precisely derived. See e.g., the summary table in (Jenniskens P. et al, 2012).

**Traditional method**

Corrections for the Earth's gravitational influence upon a meteor's direction were first proposed by Schiaparelli during the second half of nineteenth century. And since its introduction it has been widely used. . Detailed analysis of this technique was performed in (Andreev, 1990) and, in a numerical simulation, by (Gural, 2001). The influence of gravity on the zenith distance and velocity of the meteoroid is described as follows:

$$Z = Z' + \Delta Z\,, \tag{1}$$

$$\Delta Z = 2\arctan\left[\frac{V - V_g}{V + V_g} tg\left(\frac{Z'}{2}\right)\right], \tag{2}$$

$$V_g^{\,2} = V^2 - \frac{2GM_\oplus}{R_\oplus + h}. \tag{2}$$

Where $Z$ - the true zenith distance, $Z'$ - the apparent zenith distance, $V$ -the apparent velocity of meteoroid, $V_g$ - geocentric velocity of meteoroid, $GM_\oplus$ - geocentric gravitational constant, $R_\oplus$ - the Earth's mean radius, $h$ - a beginning height of a meteor. The zenith attraction method applies these corrections for zenith distance and velocity.

Next, the diurnal aberrations are taken into account and the velocity components are transformed to the inertial coordinate system. Finally, the position and velocity of the Earth, relative to the Sun, is calculated. Earth's position is taken as the position of the meteoroid, corrected to its atmospheric intercept point, in a heliocentric coordinate system, and the components of the meteoroid's velocity are added to the components of the Earth's velocity. The calculated heliocentric state vector of the meteoroid may be then be transformed into the orbital elements. As will be shown below, the traditional technique works well for fast meteoroids, but may give errors for low-velocity meteors. As calculated from the Eqs. (1-3), both the velocity and the zenith distance of the meteoroid are continuously changing as the meteoroid approaches Earth.

**Method description**

In contrast to the zenith attraction method, as discussed above, our study employs strict transformations of coordinate systems and velocity vectors recommended by the IAU International Earth Rotation and Reference Systems Service in the IERS Conventions (2010), see

(Petit & Luzum, 2010), (SOFA, 2013) and a backward numerical integration (Plakhov, Y., et al, 1989) of the equations of motion.

As a first step, we transform the velocity components from the topocentric horizontal coordinate system to the Greenwich equatorial coordinate system:

$$\begin{pmatrix} Vx \\ Vy \\ Vz \end{pmatrix} = \mathbf{M}^{\mathbf{T}} \begin{pmatrix} Vn \\ Ve \\ Vu \end{pmatrix}, \tag{3}$$

$$\mathbf{M} = \mathbf{Q_1}\mathbf{R}_2(\phi - 90°)\mathbf{R}_3(\lambda), \tag{4}$$

where *Vn, Ve, Vu* and *Vx, Vy, Vz* are components of the velocity of a meteor in the topocentric horizontal and in the Greenwich equatorial coordinate systems, respectively, matrix $\mathbf{M}^{\mathbf{T}}$ is rotation matrix from the topocentric horizontal to the Greenwich equatorial coordinate systems. $\mathbf{R_2}$, $\mathbf{R_3}$ and $\mathbf{Q_1}$ are appropriate rotation matrices and a mirror matrix, respectively, and $\varphi$ and $\lambda$ are the geodetic latitude and longitude of the initial point of the meteor.

Next, the diurnal aberration is taken into account as:

$$\begin{pmatrix} \Delta Vx \\ \Delta Vy \\ \Delta Vz \end{pmatrix} = -\omega_e \begin{pmatrix} (N+h)\cos\phi\sin\lambda \\ (N+h)\cos\phi\cos\lambda \\ 0 \end{pmatrix}, \tag{5}$$

where *h* is geodetic height, *N* is radius of curvature of Earth ellipsoid prime vertical:

$$N = R_e \Big/ \sqrt{1 - e^2 \sin^2 \varphi}, \tag{6}$$

where $R_\oplus$ is the equatorial radius of the Earth and $\omega_\oplus$ is the angular rotation velocity of the Earth.

Therefore, apparent geocentric velocity components $Vx_{geo}$, $Vy_{geo}$, $Vz_{geo}$ are

$$\begin{pmatrix} Vx_{geo} \\ Vy_{geo} \\ Vz_{geo} \end{pmatrix} = \begin{pmatrix} Vx \\ Vy \\ Vz \end{pmatrix} + \begin{pmatrix} \Delta Vx \\ \Delta Vy \\ \Delta Vz \end{pmatrix} \tag{7}$$

The transformation of the geocentric radius vector of the meteor's entry point and contributed components of the Earth's velocity from an Earth fixed, geocentric coordinate system ITRF2000, to a Geocentric Celestial Reference System (GCRS), version ICRF2 (J2000), are conducted according to the IERS Conventions (2010) (SOFA, 2013). The general formulas describing this transformation are given below. For the velocity vector:

$$\begin{pmatrix} Vx_{in} \\ Vy_{in} \\ Vz_{in} \end{pmatrix} = \mathbf{R}^{\mathbf{T}} \begin{pmatrix} Vx_{geo} \\ Vy_{geo} \\ Vz_{geo} \end{pmatrix}, \tag{8}$$

and for the geocentric radius vector of entry point, which is also the starting point of further integration:

$$\begin{pmatrix} X_{in} \\ Y_{in} \\ Z_{in} \end{pmatrix} = \mathbf{R}^{\mathbf{T}} \begin{pmatrix} X_{geo} \\ Y_{geo} \\ Z_{geo} \end{pmatrix}. \tag{9}$$

The rotation matrix **R**, defined in Eqs. (9-10) is as follows:

$$\mathbf{R = PN\Pi S}, \tag{10}$$

where and $(X_{geo}, Y_{geo}, Z_{geo},)^{\mathrm{T}}$ and $(Vx_{geo}, Vy_{geo}, Vz_{geo},)^{\mathrm{T}}$ are position and velocity vectors in geocentric ITRF coordinate system; $(X_{in}, Y_{in}, Z_{in},)^{\mathrm{T}}$ and $(Vx_{in}, Vy_{in}, Vz_{in},)^{\mathrm{T}}$ are position and velocity vectors in inertial GCRS coordinate system. **P** is the precession matrix, **N** is the nutation matrix, **Π** is the polar motion matrix, and **S** is the apparent Greenwich Sidereal Time matrix. The contributions from polar motion and high order nutation are negligible in comparison to observational errors of the meteor, so these effects can be neglected when determining a meteoroid's orbit.

The next step involves using the numerical ephemerides, DE421, distributed by the Jet Propulsion Laboratory (Folkner, Williams, & Boggs, 2009), to obtain the coordinates and velocity components of Earth at the time of occurrence of a meteor. In addition to the meteor's starting point coordinates in the inertial frame with heliocentric coordinates of the Earth, we also obtain the heliocentric position of the meteoroid. The meteoroid's heliocentric state vector at the starting point of meteor can be represented as:

$$\bar{\mathbf{r}}_{J2000} = \overline{\mathbf{R}}_{\oplus} + \overline{\mathbf{R}}_{in}, \tag{11}$$

$$\dot{\bar{\mathbf{r}}}_{J2000} = \overline{\mathbf{V}}_{\oplus} + \overline{\mathbf{V}}_{in}. \tag{12}$$

Thus, we have the initial conditions for the integration of differential equations of motion of the meteoroid. These equations of motion are as follows:

$$\ddot{\bar{\mathbf{r}}} = -\frac{GM_{sun}}{r^3}\bar{\mathbf{r}} + \ddot{\bar{\mathbf{r}}}_{Earth}(C_{nm}, S_{nm}, \bar{\mathbf{r}}, t) + \ddot{\bar{\mathbf{r}}}_{Moon}(\bar{\mathbf{r}}, t) + \sum \ddot{\bar{\mathbf{r}}}_{planets}(\bar{\mathbf{r}}, t) + \ddot{\bar{\mathbf{r}}}_{atm}(\bar{\mathbf{r}}, t). \tag{13}$$

The equations (14) are ordinary differential second order equations of a perturbed two-body problem. The right of the equations include the attraction of the central body, i.e., the Sun,

the perturbations caused by the attraction of the Earth (including its non-central gravitational field), by the Moon, the perturbations from the other planets of the solar system, and the effects of the atmospheric drag. Perturbation forces from the point mass of Earth, the Moon and the planets, as well as the none-central part of Earth's gravitational field are well known and widely used. For instance, an accounting for these perturbation forces is presented in (Montenbruck & Gill, 2000).

The meteoroid term of deceleration in upper atmosphere may be calculated using the following expression:

$$\ddot{\vec{r}}_{atm} = -\frac{1}{2} c_d \rho_{atm} \frac{S}{M} V_{rel} \overline{\mathbf{V}}_{rel}, \qquad (14)$$

where $V_{rel}$ is meteoroid velocity relative the atmosphere, $c_d$ –drag coefficient, $S/M$ – cross section to mass ratio. Here we are taking into account only the drag component and we use the USA 1976 Standard Atmosphere model (Standard Atmosphere, 1976) to estimate the atmospheric drag effect at heights up to 86 km. For altitudes higher than 86 km and lower than 150 km, the NRLMSISE-00 model (Picone, J., et al., 2002) was used. An estimation of the atmospheric drag influence on the orbit of the Košice meteoroid, which had an entry height of about 68.3 km, is presented in the table 1. For integrations deep into the past, the perturbations of the other planets need to be taken into consideration as the planets become the main source of perturbations.

For the integration of equations of motion (14) high order implicit single-sequence methods up to the 23$^{rd}$ order is used (Plakhov, Y., et al, 1989). The equations are integrated back in time up to the intersection of the meteoroid's orbit with the Hill sphere of the Earth. Thus the obtained orbit of the meteoroid is not distorted by the attraction of the Earth and Moon.

A similar approach was used in (Zuluaga, Ferrin, & Geens, 2013) to determine the orbit of the Chelyabinsk meteorite, where the integration of the equations of motion was done using the software package, "mercury6" (Chambers, 1999). The program was designed for the numerical solution of the n-body problem. In another study, (Clark & Wiegert, 2011), the authors compared Ceplecha's analytical orbit determination method (Ceplecha, 1987), with the results of their own numerical integration, which demonstrated close agreement between both approaches. Backward numerical integration is widely used for analysis of dynamical origin of meteoroids. In the recent past several authors conducted an analysis of the dynamical evolution of asteroid or meteoroid's orbits, see e.g. (Madiedo et. al. 2013, 2014).

**Error propagation**

The strict estimation of the derived uncertainties of the derived meteoroid's orbit is a rather complicated multistep process. Critical to this process is the propagation of uncertainties

from the initial data: the apparent radiant, the velocity and coordinate of entry point, and the time of entry to the covariance matrix of meteoroid orbital elements outside the Hill sphere. For example, some authors obtained this covariance matrix by using the method of finite difference. They calculated the uncertainties of the orbit by changing the initial data and then recalculated the orbit. Thus, the orbit uncertainties estimation is performed by the differences in the resulting orbits, which was calculated with different initial conditions (Bettonvil, 2006).

In our work, we consider another approach, that of using strict covariance transformations. This method is based on the use of strict formulas and, accordingly, has less calculation overhead, but its mathematical expression is quite cumbersome.

As initial data we have the topocentric radiant (*A*, *El*), the apparent entry velocity (*V*), the geodetic coordinates ($\varphi$, $\lambda$, *h*) of entry point and the moment ($t_e$) of entry into the atmosphere and its dispersions. As result we have to obtain covariance matrices of state vector ( $\overline{\mathbf{r}}, \dot{\overline{\mathbf{r}}}$ ,) and orbital elements (*a, e, i,* $\Omega$, $\omega$, *M*).

Let's write a general rule for covariance transformation (Rice, 2006).

Suppose that we have two random vectors $\overline{\mathbf{Y}}$ and $\overline{\mathbf{X}}$ , associated with vector transformation *F*:

$$\overline{\mathbf{Y}} = F(\overline{\mathbf{X}}). \tag{15}$$

Accordingly, covariance matrices **CovY** and **CovX** of vectors $\overline{\mathbf{Y}}$ and $\overline{\mathbf{X}}$, are connected by:

$$\mathbf{CovY} = \mathbf{J} \cdot \mathbf{CovX} \cdot \mathbf{J}^{\mathbf{T}}, \tag{16}$$

where matrix $\mathbf{J}_{n,\,m} = \dfrac{\partial F_n}{\partial X_m}$ is a partial derivatives matrix of vector-valued function, *F*, the so-called Jacobi matrix.

For the first step, we transform dispersions of topocentric radiant from the spherical to Cartesian coordinates by using well known matrix:

$$\mathbf{P}_{AhV \to NEU} = \frac{\partial(V_n, V_e, V_u)}{\partial(V, A, El)}, \tag{17}$$

$$\mathbf{P}_{AhV \to NEU} = \begin{pmatrix} \cos El \cdot \cos A & -V \cos El \cdot \sin A & -V \sin El \cdot \cos A \\ \cos El \cdot \sin A & V \cos El \cdot \cos A & -V \sin El \cdot \sin A \\ \sin El & 0 & V \cos El \cdot \end{pmatrix}, \tag{18}$$

$$\mathbf{Cov}_{NEU} = \mathbf{P}_{AhV->NEU}\ \mathbf{Cov}_{AzhV} \mathbf{P}^{\mathbf{T}}_{AhV->NEU}. \tag{19}$$

Then topocentric Cartesian covariance matrix is transformed from a local horizontal coordinate system to the geocentric Greenwich equatorial coordinate frame ITRF2000 by using rotation matrix **M** (8):

$$\mathbf{Cov}_{VITRF} = \mathbf{M}\,\mathbf{Cov}_{NEU}\mathbf{M}^{\mathbf{T}}. \quad (20)$$

From the other way we convert dispersion of entry point coordinates from geodetic ellipsoidal ($\varphi$, $\lambda$, $h$) to Cartesian geocentric ITRF coordinates. The transition matrix was obtained from differentiation following equation from $\varphi$, $\lambda$, $h$:

$$\begin{aligned} X_{ITRF} &= (N+h)\cos\varphi\cos\lambda \\ Y_{ITRF} &= (N+h)\cos\varphi\sin\lambda \\ Z_{ITRF} &= (N(1-e^2)+h)\sin\varphi \end{aligned}, \quad (21)$$

where $N$ is radius of curvature of Earth ellipsoid prime vertical (6), $R_e$ is equatorial radius of Earth ellipsoid and $e$ is its eccentricity.

$$\mathbf{P}_{\varphi,\lambda,h\to ITRF} = \frac{\partial(X,Y,Z)_{ITRF}}{\partial(\varphi,\lambda,h)}, \quad (22)$$

$$\mathbf{P}_{\phi,\lambda,h\to ITRF} = \begin{pmatrix} -(M+h)\sin\varphi\cdot\cos\lambda & (N+h)\cos\varphi\cdot\sin\lambda & \cos\varphi\cdot\cos\lambda \\ -(M+h)\sin\varphi\cdot\sin\lambda & (N+h)\cos\varphi\cdot\cos\lambda & \cos\varphi\cdot\sin\lambda \\ (M+h)\cos\varphi & 0 & \sin\varphi \end{pmatrix}, \quad (23)$$

$$\mathbf{Cov}_{XITRF} = \mathbf{P}_{\phi,\lambda,h\to ITRF}\,\mathbf{Cov}_{\phi,\lambda,h}\mathbf{P}^{\mathbf{T}}_{\phi,\lambda,h\to ITRF}, \quad (24)$$

where $M$ is radius of curvature of Earth ellipsoid meridian:

$$M = R_e(1-e^2)\Big/\sqrt{(1-e^2\sin^2\varphi)^3} \quad (25)$$

After that, we compose two 3x3 dimension covariance matrices of position and velocity to 6x6 covariance matrix of meteoroid state vector, $\mathbf{Cov}_{ITRF.}$

Next, the covariance matrix of the ITRF coordinates and velocity are transformed into the true equinox coordinate system using the matrix $\mathbf{P}_{ITRF\to TEQ}$:

$$\mathbf{Cov}_{TEQ} = \mathbf{P}_{ITRF\to TEQ}\,\mathbf{Cov}_{ITRF}\mathbf{P}^{\mathbf{T}}_{ITRF\to TEQ}. \quad (26)$$

Matrix $\mathbf{P}_{ITRF\to TEQ}$ has a block structure:

$$\mathbf{P}_{ITRF\to TEQ} = \begin{pmatrix} \mathbf{S} & 0 \\ \dot{\mathbf{S}} & \mathbf{S} \end{pmatrix}, \quad (27)$$

here **S** is a matrix of sidereal time. Explicit forms of these matrices are:

$$\mathbf{S} = \begin{pmatrix} \cos S & \sin S & 0 \\ -\sin S & \cos S & 0 \\ 0 & 0 & 1 \end{pmatrix}, \quad (28)$$

$$\dot{\mathbf{S}} = \frac{dS}{dt} \cdot \begin{pmatrix} -\sin S & \cos S & 0 \\ -\cos S & -\sin S & 0 \\ 0 & 0 & 0 \end{pmatrix}, \qquad (30)$$

here $S$ is Greenwich sidereal time, and its first derivatives is equal to Earth rotation rate $dS/dt = \omega_{\oplus}$.

Also, we have to take into account error of the Earth attitude $\delta_{EA}$ due the time registration error:

$$\delta_{EA}^2 = \left( \frac{d}{dt} \mathbf{P}_{ITRF \to TEQ} \cdot \begin{pmatrix} \bar{\mathbf{r}}_{ITRF} \\ \dot{\bar{\mathbf{r}}}_{ITRF} \end{pmatrix} \right)^2 \delta t^2, \qquad (29)$$

Squares of errors of Earth attitude are added to diagonal elements of state vector covariance matrix. Further, we transform covariance matrix from true equinox to inertial coordinate system of the reference epoch J2000.0. For this transformation, we use precision and nutation matrices – **P** and **N**, respectively, which were mentioned previously (10).

$$\mathbf{Cov}_{J2k} = (\mathbf{PN})\, \mathbf{Cov}_{TEQ} (\mathbf{PN})^{\mathbf{T}}. \qquad (30)$$

Then, the transformation from an equatorial to an ecliptic coordinate system is performed by counter-clockwise rotation of coordinate frame around $X$-axis to ecliptic obliquity angle $\varepsilon$:

$$\mathbf{Cov}_{EJ2k} = \mathbf{R}_1(\varepsilon)\ \mathbf{Cov}_{J2k} \mathbf{R}_1^{\mathbf{T}}(\varepsilon). \qquad (31)$$

After that, we have to take into account errors of position and velocity of Earth caused by the time registration error:

$$\begin{aligned} \delta \bar{\mathbf{R}}_{Earth}^2 &= \dot{\bar{\mathbf{R}}}_{Earth}^2 \delta t^2, \\ \delta \dot{\bar{\mathbf{R}}}_{Earth}^2 &= \ddot{\bar{\mathbf{R}}}_{Earth}^2 \delta t^2, \end{aligned} \qquad (32)$$

here $\bar{\mathbf{R}}_{Earth}$ - vector of Earth's heliocentric position, $\dot{\bar{R}}_{Earth}$ - vector of Earth's orbital velocity, $\ddot{\bar{\mathbf{R}}}_{Earth}$ - Earth's acceleration vector, which can be computed from equations of two body problem:

$$\ddot{\bar{\mathbf{R}}}_{Earth} = -GM_{Sun} \frac{\bar{\mathbf{R}}_{Earth}}{R_{Earth}^3}. \qquad (33)$$

Errors computed from equations (32) must be added to diagonal elements of geocentric inertial state vector covariance matrix. In this way, we obtain the covariance matrix of heliocentric inertial state vector at the epoch of entry to the atmosphere.

If the selected interval of integration is rather long, then we have to propagate a covariance matrix from the entry epoch then backward to the epoch marking the end of the

backward integration. . For this transition a matrix of derivatives of the state vector at epoch *t* by state vector at epoch $t_0$ should be computed:

$$\mathbf{\Phi}_{t_0 \to t} = \frac{\partial(x, y, z, \dot{x}, \dot{y}, \dot{z})_t}{\partial(x, y, z, \dot{x}, \dot{y}, \dot{z})_{t_0}}. \tag{34}$$

The so-called, state transition matrix or "matrix of isochronous derivatives" is employed next. There are many ways to compute this matrix. We use a technique based on the integration of variation equations, a method detailed and described in (Montenbruck & Gill, 2000):

$$\ddot{\mathbf{\Phi}}(t) = \frac{\partial \ddot{\mathbf{r}}}{\partial \mathbf{r}} \mathbf{\Phi}(t) + \frac{\partial \ddot{\mathbf{r}}}{\partial \dot{\mathbf{r}}} \dot{\mathbf{\Phi}}(t). \tag{35}$$

We use this method because it is a reasonable compromise between the computational loading of finite differences methods on the one hand, and the complicated formulas of analytical solution on the other hand. Furthermore, there are second order ordinary differential equations, like the equation (13), consequently, joint integration of system (13) and (35) are rather suitable for algorithmic realization. Matrices of partial derivatives $\frac{\partial \ddot{\mathbf{r}}}{\partial \mathbf{r}}$ and $\frac{\partial \ddot{\mathbf{r}}}{\partial \dot{\mathbf{r}}}$ are computed analytically. For errors propagation we optionally can use the accelerations from the Sun, Earth and the Moon. Thus, the state transition matrix is calculated in accordance with the selected force model. Explicit expressions for these derivatives are given in (Montenbruck & Gill, 2000).

By using this method, we can obtain the covariance matrix at any epoch prior to the meteoroid's entry into the atmosphere:

$$\mathbf{Cov}_{EJ2k}(t) = \mathbf{\Phi}_{t_0 \to t}\ \mathbf{Cov}_{EJ2k}(t_0) \mathbf{\Phi}^{\mathbf{T}}_{t_0 \to t}. \tag{36}$$

The last step in the covariance propagation is the calculation of the standard deviation of the orbital elements at epoch *t*, using a matrix of partial derivatives of the Keplerian orbital elements with respect to the state vector:

$$\mathbf{E} = \frac{\partial(a, e, i, \Omega, \omega, M)}{\partial(x, y, z, \dot{x}, \dot{y}, \dot{z})}, \tag{37}$$

$$\mathbf{Cov}_{OEJ2k}(t) = \mathbf{E}\, \mathbf{Cov}_{EJ2k}(t) \mathbf{E}^{\mathbf{T}}. \tag{38}$$

Methods to compute the matrix, **E, are** also given in detail in (Montenbruck & Gill, 2000).

Summarizing, this is the approach we implemented to estimate a meteoroid's orbital accuracy using the uncertainties of the topocentric radiant and the coordinates of point of the meteoroid's entry into the atmosphere.

**Application to the recent data obtained by the Finnish Fireball Network**

We applied the orbit determination method described above to selected fireballs recorded over recent years by the Finnish Fireball Network (FFN). Currently, the network consists of the 24 active stations with permanent instrumental setups. The FFN monitors an area over Finland and neighboring regions covering, in total, an area of about 400.000 $km^2$ (Gritsevich, et al., 2014b). A majority of the interesting captured events are reduced over the following days of their registration. The atmospheric trajectories corresponding to the visual path of fireballs are reproduced on a case-by-case basis using the fb_entry program (Lyytinen & and Gritsevich, 2013).

For orbit determination, we have selected the Oijärvi (FN20101226), Mikkeli (FN20130913), Annama (FN20140419), and the Haapavesi (FN20140925) fireballs. The reconstruction of the trajectory for each of these fireballs was done in great detail and used real time atmospheric data for even greater accuracy (Lyytinen & Gritsevich, 2015).

The Oijärvi fireball was observed by two FFN stations using three cameras. Unfortunately, the stations were located relatively close to each other. The trajectory was however successfully reconstructed except for the very end of the luminous track.

The Mikkeli fireball was observed by four FFN stations using five cameras. The resulting data are quite reliable, though the initial mass of the meteoroid was relatively small (Lyytinen & Gritsevich, 2015).

The Annama fireball was observed by three FFN stations and led to successful meteorite recovery at the end of May 2014 (Gritsevich et al. 2014b; Trigo-Rodriguez, et al., 2015). A dashcam video of the Annama fireball made by Alexandr Nesterov from Snezhnogorsk was a valuable asset in the trajectory reconstruction.

The Haapavesi event was a low entry angle fireball lasting for about 21 seconds. It was well captured by one FFN camera (Figure 1). This one station observation was in turn, supported by using the accurate infrasound timing data from the Swedish Jämtön station and by additional data from six Finnish seismic stations. As a result, its entry track was reconstructed with good precision. The input and output data and differences with traditional approach for the selected fireballs are summarized in the table 1.

Table 1. Orbits of meteoroids registered by FFN calculated by using zenith attraction approach and by our proposed approach.

Initial data.

| ***Name (ID)*** | | ***$t_e$*** | ***$\varphi$,°*** | ***$\lambda$, °*** | ***$h_e$,km*** | ***Az, deg*** | ***El, deg*** | ***$V_e$, km/s*** |
|---|---|---|---|---|---|---|---|---|
| Oijärvi | Values | 2010-12-26 14:06:09.0 | 64.78 | 26.91 | 77.00 | 156.20 | 25.80 | 13.80 |

| | | | | | | | | |
|---|---|---|---|---|---|---|---|---|
| (FN20101226) | RMS | 5.00 sec | 0.02 | 0.01 | 1.00 | 0.30 | 0.30 | 1.00 |
| Mikkeli | Values | 2013-09-13 22:33:47.0 | 61.46 | 26.90 | 82.10 | 238.94 | 55.06 | 14.98 |
| (FN20130913) | RMS | 1.00 sec | 0.01 | 0.01 | 0.50 | 0.40 | 0.20 | 0.10 |
| Annama | Values | 2014-04-19 22:14:09.3 | 67.93 | 30.76 | 83.90 | 176.10 | 34.32 | 24.21 |
| (FN20140419) | RMS | 0.50 sec | 0.01 | 0.01 | 0.50 | 0.50 | 0.50 | 0.50 |
| Haapavesi | Values | 2014-09-25 3:12:15.0 | 66.52 | 25.16 | 70.95 | 357.25 | 11.05 | 14.78 |
| (FN20140925) | RMS | 1.00 sec | 0.03 | 0.02 | 1.00 | 0.30 | 0.30 | 0.30 |

Meteoroid orbits computed using proposed method

| ***Name (ID)*** | **Epoch, UTC** | | ***a, a.u.*** | ***e*** | ***i, °*** | ***Ω, °*** | ***ω, °*** | ***M, °*** |
|---|---|---|---|---|---|---|---|---|
| Oijärvi | 2010-12-23 | Orbital elements | 2.4582 | 0.6011 | 2.8018 | 94.5264 | 352.7669 | 0.6752 |
| (FN20101226) | 14:06:09.0 | RMS | 0.5115 | 0.0830 | 0.2184 | 0.0002 | 0.2761 | 0.2940 |
| Mikkeli | 2013-09-10 | Orbital elements | 1.4351 | 0.3652 | 12.2118 | 171.1336 | 229.6707 | 335.2453 |
| (FN20130913) | 22:33:47.0 | RMS | 0.0114 | 0.0053 | 0.1324 | 0.0004 | 0.3035 | 0.4456 |
| Annama | 2014-04-14 | Orbital elements | 2.0004 | 0.6817 | 14.8276 | 29.5868 | 264.4220 | 342.5477 |
| (FN20140419) | 22:14:09.3 | RMS | 0.1069 | 0.0180 | 0.5036 | 0.0005 | 1.1035 | 1.6363 |
| Haapavesi | 2014-09-22 | Orbital elements | 2.5301 | 0.6042 | 9.2407 | 181.8271 | 174.6757 | 0.3044 |
| (FN20140925) | 3:12:15.0 | RMS | 0.1107 | 0.0173 | 0.3510 | 0.0017 | 0.3129 | 0.0632 |

Meteoroid orbits computed using traditional method

| ***Name (ID)*** | ***Epoch, UTC*** | | ***a, a.u.*** | ***e*** | ***i, °*** | ***Ω, °*** | ***ω, °*** | ***M, °*** |
|---|---|---|---|---|---|---|---|---|
| Oijärvi | 2010-12-23 | Orbital elements | 2.4630 | 0.6020 | 2.7550 | 94.5150 | 352.5133 | 0.7273 |
| (FN20101226) | 14:06:09.0 | RMS | 0.5160 | 0.0834 | 1.4265 | 0.0096 | 0.9182 | 0.5695 |
| Mikkeli | 2013-09-10 | Orbital elements | 1.4366 | 0.3650 | 12.1240 | 171.1133 | 229.3388 | 335.4228 |
| (FN20130913) | 22:33:47.0 | RMS | 0.0130 | 0.0058 | 0.1395 | 0.0001 | 0.4006 | 0.5047 |
| Annama | 2014-04-14 | Orbital elements | 2.0026 | 0.6819 | 14.8057 | 29.5837 | 264.3719 | 342.5833 |
| (FN20140419) | 22:14:09.3 | RMS | 0.1104 | 0.0180 | 0.6404 | 0.0005 | 1.4850 | 1.6030 |
| Haapavesi | 2014-09-22 | Orbital elements | 2.5251 | 0.6033 | 9.2190 | 181.7975 | 174.9650 | 0.2555 |
| (FN20140925) | 3:12:15.0 | RMS | 0.1784 | 0.0281 | 0.4981 | 0.0005 | 0.3202 | 0.1161 |

Differences between orbits computed using proposed and traditional methods

| ***Name (ID)*** | ***Epoch, UTC*** | ***a, a.u.*** | ***e*** | ***i, °*** | ***Ω, °*** | ***ω, °*** | ***M, °*** |
|---|---|---|---|---|---|---|---|
| Oijärvi (FN20101226) | 2010-12-26 14:06:09.0 | -0.0048 | -0.0009 | 0.0468 | 0.0114 | 0.2536 | -0.0521 |
| Mikkeli (FN20130913) | 2013-09-13 22:33:47.0 | -0.0015 | 0.0002 | 0.0878 | 0.0204 | 0.3319 | -0.1775 |
| Annama (FN20140419) | 2014-04-19 22:14:09.3 | -0.0022 | -0.0002 | 0.0218 | 0.0031 | 0.0501 | -0.0356 |
| Haapavesi (FN20140925) | 20140925 3:12:15.0 | 0.0051 | 0.0009 | 0.0217 | 0.0296 | -0.2893 | 0.0488 |

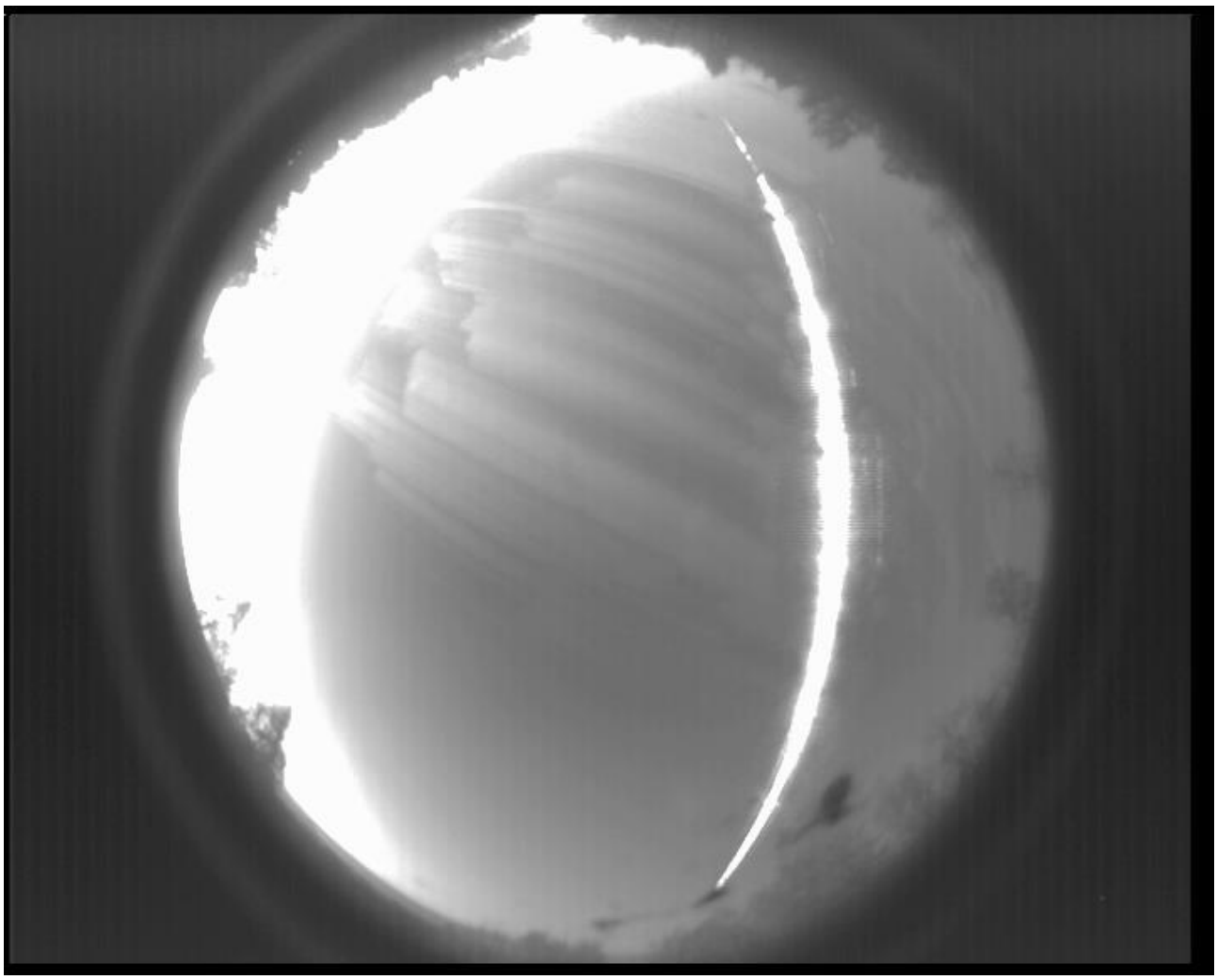

Figure 1. The Haapavesi (FN20140925) fireball imaged by Pekka Kokko in Muhos station belonging to the Finnish Fireball Network.

**Results and Discussion**

Our method of determining a meteoroid's orbit, as discussed above, was implemented into the software package called "Meteor Toolkit" which runs on a Windows operating system (see Appendix 2 for system requirements). The graphical user interface (GUI), of this application is shown at the figures in the Appendix 3.

The software allows the researcher to effectively and accurately process observational data in an automated mode. The software can output a meteoroid's pre-impact orbit, perform an analysis of the orbital motion of the meteoroid prior to the impact with the Earth, and possibly assist in the identification of the origin or the parent body of the meteoroid. The software also makes it possible to estimate a probable location of the meteorite's fall site (when applicable) by following the numerical integration of the equations of motion (Brown P., et al, 2011) to the intersection with the surface of the Earth.

Table 2 presents selected results derived by using the Meteor Toolkit software (labeled "This study" in Table 2). Our results are compared in turn to the orbital calculations for several well-studied meteorite falling events that were previously published. It should be noted that the authors of each study (Table 2 top most columns 3-8) used their own unique modified implementations of the zenith attraction model discussed in the introduction. The results obtained using our method compared favorably to the cited orbits.

Table 2. Comparison of orbits calculated by the authors using traditional approach with orbits obtained by numerical integration of equations of motion in this study.

| | *Name* | *Buzzard Coulee* (Milley, 2010) | *Grimsby* (Brown P., et al, 2011) | *Neuschwanstein* (Spurny, Oberst, & Heinlein, 2003) | *Sutter's Mill* (Jenniskens P. et al, 2012) | *Chelyabinsk* (Popova, O.P., Jenniskens, P. et al., 2013) | *Košice* (Borovicka J., et al., 2013) |
|---|---|---|---|---|---|---|---|
| *Topocentric radiant* | Epoch, UT | 2008-11-21 00:26:43.0±1.0 | 2009-09-25 01:02:58.4±0.3 | 2000-04-06 20:20:17.7 | 2012-04-22 14:51:12.8±1.1 | 2013-02-15 03:20:20.8±0.1 | 2010-02-28 22:24:47.0 |
| | B, ° | 53.169±0.001 | 43.534±0.001 | 47.3039±0.0006 | 38.803± | 54.445±0.018 | 48.467±0.021 |
| | L, ° | -10.059±0.001 | -80.194±0.001 | 11.5524±0.0009 | -120.908± | 64.565±0.030 | 20.705±0.011 |
| | H, km | 63.8±0.7 | 100.5±0.1 | 84.950±0.95 | 90.2±0.4 | 97.1±1.6 | 68.3±1.4 |
| | $A_{app}$, ° | 347.5±0.4 | 309.40±0.19 | 125.000±0.03 | 92.5±0.4 | 103.2±0.4 | 252.6±4.0 |
| | $h_{app}$, ° | 66.7±0.4 | 55.20±0.13 | 49.75±0.03 | 26.3±0.6 | 18.30±0.4 | 58.8±2.0 |
| | $V_{app}$, km/s | 18.0±0.4 | 20.910±0.19 | 20.950±0.04 | 28.6±0.6 | 19.160±0.30 | 15.0±0.3 |
| *Published orbit* | A, a.u. | 1.25±0.02 | 2.04±0.05 | 2.40±0.02 | 2.59±0.35 | 1.76±0.16 | 2.71±0.24 |
| | e | 0.23 ± 0.02 | 0.518±0.011 | 0.670±0.002 | 0.824±0.020 | 0.581±0.018 | 0.647±0.032 |
| | i, ° | 25.0 ± 0.8 | 28.07±0.28 | 11.418±0.03 | 2.38±1.16 | 4.93±0.48 | 2.0±0.8 |
| | Ω, ° | 238.93739 ± 0.00008 | 182.9561 | 16.82664±0.00001 | 32.774±0.06 | 326.4422±0.0028 | 340.072±0.004 |
| | ω, ° | 211.3 ± 1.4 | 159.865±0.43 | 241.208±0.06 | 77.8±3.2 | 108.3±3.8 | 204.2±1.2 |
| *This study* | Epoch, UT | 2008-11-18 00:26:43.0 | 2009-09-22 01:02:58.40 | 2000-04-03 20:20:17.7 | 2012-04-19 14:51:12.8 | 2013-02-12 03:20:20.8.0 | 2010-02-25 22:24:47.0 |
| | A, a.u. | 1.231±0.024 | 2.026±0.039 | 2.397±0.013 | 2.421±0.196 | 1.760±0.043 | 2.725±0.225 |
| | e | 0.219±0.014 | 0.516±0.009 | 0.669±0.002 | 0.816±0.017 | 0.580±0.012 | 0.649±0.029 |
| | i, ° | 25.186±0.626 | 28.088±0.24 | 11.594±0.025 | 2.717±0.607 | 4.991±0.277 | 2.015±0.903 |
| | Ω, ° | 238.94997±0.00031 | 181.98433±0.00009 | 16.83654±0.00003 | 32.77001±0.01461 | 326.45423±0.00164 | 340.14579±0.0310 |
| | ω, ° | 211.377±1.409 | 159.070±0.304 | 241.198±0.06 | 75.997±0.974 | 108.200±0.722 | 204.108±1.575 |
| | M, ° | 337.837±1.604 | 4.782±0.208 | 348.584±0.107 | 10.831±1.471 | 17.855±0.825 | 355.333±0.734 |
| *Differences* | A, a.u. | 0.019 | 0.014 | 0.003 | 0.169 | 0.000 | -0.015 |
| | e | 0.011 | 0.002 | 0.001 | 0.008 | 0.001 | -0.002 |
| | i, ° | -0.186 | -0.018 | -0.176 | -0.337 | -0.061 | -0.015 |
| | Ω, ° | -0.01258 | 0.97177 | -0.0099 | 0.00399 | -0.01203 | -0.07579 |
| | ω, ° | -0.077 | 0.795 | 0.010 | 1.803 | 0.100 | 0.092 |

Meteor Toolkit also incorporates routines that analyze the contributions of certain perturbations to the resulting meteoroid's orbit. In Table 2, the effects of perturbations from the non-central part of Earth's gravity field to the second degree and order, and the attraction from the Moon upon the orbits of several well studied meteoroids are demonstrated. Integration was carried out to the upper boundary of Earth's atmosphere and to an epoch of 4 days prior to the impact.

In Table 2 we can see that the difference between the traditional, i.e. zenith attraction approach, and our method, which is based on the integration of the equations of motion, depends on the pre-atmospheric velocity as well as the initial height of a meteor. The effects of perturbations on the resulting orbit are generally less than orbital elements uncertainties. The exception of this rule is the magnitude of difference on the orbits longitude of ascending node. The influences of perturbations are significant in this case, taking into account the height accuracy of this parameter.

The initial height of the Košice fireball was observed to be fairly low at 68.3 km (Borovicka J., et al., 2013). At this altitude, the atmospheric drag normally predominates over that of Earth's gravity (Gritsevich M. , 2010). Our estimation of the drag effect caused by interaction of the meteor with the Earth's atmosphere shows it is very significant at this altitude and, in particular, it may stimulate meteoroid's break-up in the atmosphere. This conclusion is supported by the large number of Kosice meteorite fragments recovered on the ground (Gritsevich et al., 2014a).

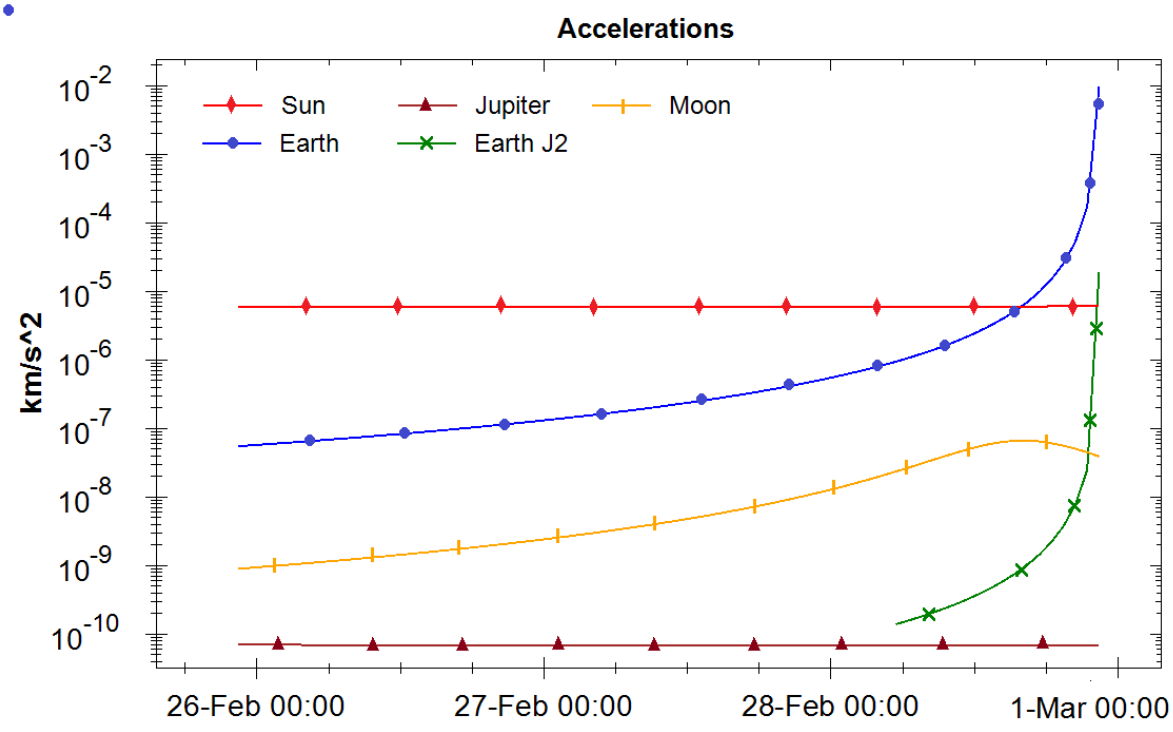


Figure 2. Gravitational acceleration in motion of the meteoroid Košice on three-day interval before the impact.

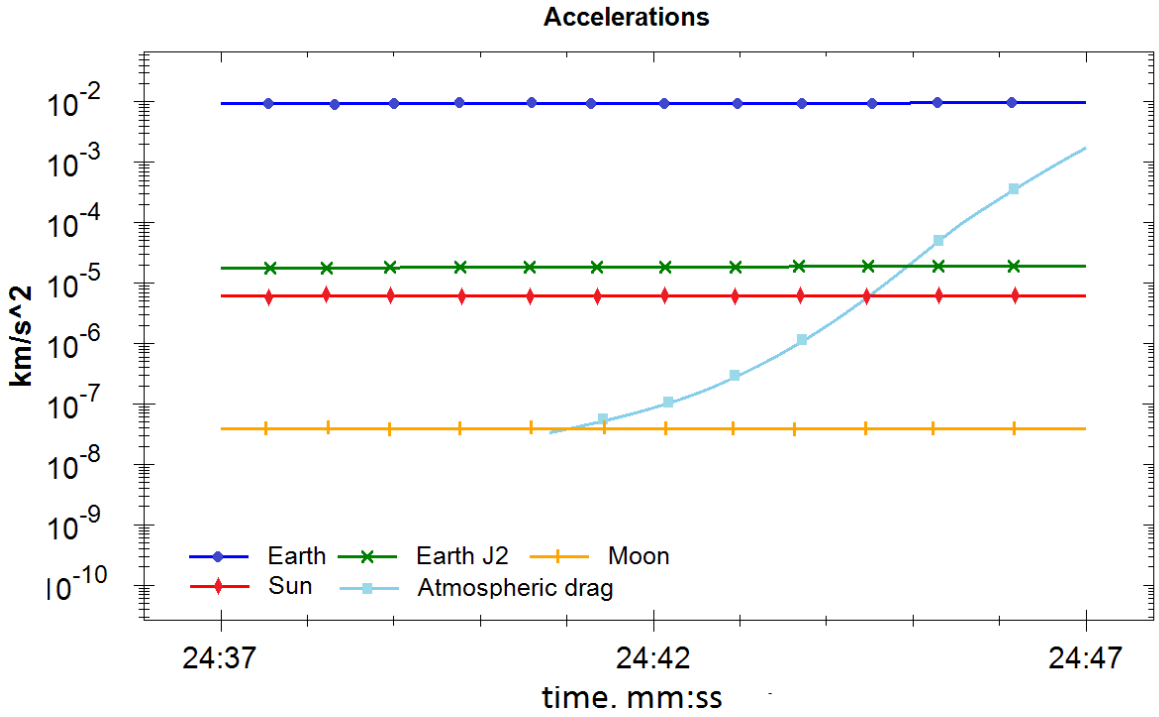


Figure 3. Acceleration in motion of the meteoroid Košice on 10 seconds before the start of visible track.

The USA 1976 model (Standard Atmosphere, 1976) describes the atmospheric parameters at altitudes from sea level up to 86 km. For higher altitudes, the atmosphere model, NRLMSISE-00, is used. Consequently, in the case of the Košice meteorite, the magnitude of perturbation caused by the atmospheric drag as expressed on the semi-major axis reaches about 0.0007 AU. When deriving the atmospheric drag we assumed an initial mass of 3500 kg, and bulk density of 3.4 g/cm$^3$ in accordance with (Kohout et al. 2014). We also supposed a spherical shape for the meteoroid. Thus, in case of Košice meteoroid, the values of this effect is much less than the influence of the observations uncertainties, consequently it is not necessary to consider the atmospheric drag effect acting on the meteoroid during its flight through the upper layers of the atmosphere.

Table 3 contains a series of comparisons of well documented, meteorite dropping, fireballs whose orbits were calculated using the zenith attraction approach, with the orbits obtained based on our numerical integration of equations of motion that are incorporated into Meteor Toolkit. The equations of motion were integrated taking into account various sources of perturbing accelerations. The initial data, which were used for orbital calculations, are shown in the second row of each meteor's table. If the difference between the orbital elements calculated with and without perturbation is less than 0.0001, then it is shown as zero. Each meteoroid's orbit was calculated at an epoch of 4 days prior to their impact with Earth. Explanations of the symbols used in the tables are given in the Appendix 1.

Table 3. Comparisons of some published meteor orbits that were calculated by using zenith attraction approach with orbits obtained by our Meteor Toolkit. For orbital computations the initial data from table 1 were used. Designation “Earth”, “J2”, “Moon”, “Atm.” are notations for the perturbations from Earth as point mass, Earth’s flattening, Moon as point mass, and atmospheric drag, respectively.

| *Orbit* | *a, a.u.* | *e* | *i, °* | *Ω, °* | *ω, °* | *M, °* |
|---|---|---|---|---|---|---|
| Košice | | | | | | |
| 1. Traditional method | 2.7101 | 0.6468 | 1.9399 | 340.1189 | 203.8906 | 355.3313 |
| 2. Earth | 2.7253 | 0.6490 | 2.0177 | 340.1454 | 204.0886 | 355.3370 |
| 3. Earth + J2 + Moon | 2.7248 | 0.6489 | 2.0154 | 340.1458 | 204.1077 | 355.3325 |
| 4. Earth + J2 + Moon + Atm. | 2.7255 | 0.6490 | 2.0158 | 340.1458 | 204.1078 | 355.3442 |
| 1.-2. | -0.0152 | -0.0022 | -0.0778 | -0.0264 | -0.1981 | -0.0057 |
| 2.-3. | 0.0005 | 0.0001 | 0.0023 | -0.0004 | -0.0191 | 0.0045 |
| 3.-4. | -0.0007 | -0.0001 | -0.0004 | 0.0000 | -0.0010 | -0.0017 |
| Standard deviation | 0.225 | 0.029 | 0.903 | 0.0310 | 1.575 | 0.734 |
| Chelyabinsk | | | | | | |
| 1. Traditional method | 1.7605 | 0.5811 | 5.0670 | 326.4416 | 108.0740 | 17.8612 |
| 2. Earth | 1.7598 | 0.5803 | 4.9900 | 326.4541 | 108.2039 | 17.8575 |
| 3. Earth + J2 + Moon | 1.7599 | 0.5804 | 4.9912 | 326.4542 | 108.2004 | 17.8552 |
| 1.-2. | 0.0007 | 0.0008 | 0.0770 | -0.0126 | -0.1298 | 0.0037 |
| 2.-3. | -0.0001 | -0.0001 | -0.0012 | -0.0001 | 0.0034 | 0.0023 |
| Standard deviation | 0.043 | 0.012 | 0.277 | 0.00164 | 0.722 | 0.825 |
| Sutters Mill | | | | | | |
| 1. Traditional method | 2.4197 | 0.8165 | 2.7546 | 32.7650 | 75.9274 | 10.8356 |
| 2. Earth | 2.4200 | 0.8163 | 2.7194 | 32.7699 | 75.9912 | 10.8355 |
| 3. Earth + J2 + Moon | 2.4206 | 0.8163 | 2.7170 | 32.7700 | 75.9975 | 10.8315 |
| 1.-2. | -0.0003 | 0.0002 | 0.0352 | -0.0049 | -0.0638 | 0.0001 |
| 2.-3. | -0.0006 | 0.0000 | 0.0024 | -0.0001 | -0.0063 | 0.0040 |
| Standard deviation | 0.196 | 0.017 | 0.607 | 0.0146 | 0.974 | 1.471 |
| Buzzard Coulee | | | | | | |
| 1. Traditional method | 1.2298 | 0.2174 | 25.1797 | 238.9419 | 211.1418 | 337.9422 |
| 2. Earth | 1.2307 | 0.2184 | 25.1840 | 238.9499 | 211.3987 | 337.8158 |
| 3. Earth + J2 + Moon | 1.2310 | 0.2186 | 25.1862 | 238.9500 | 211.3767 | 337.8372 |
| 1.-2. | -0.0010 | -0.0010 | -0.0043 | -0.0081 | -0.2569 | 0.1264 |
| 2.-3. | -0.0002 | -0.0001 | -0.0022 | 0.0000 | 0.0220 | -0.0214 |
| Standard deviation | 0.024 | 0.014 | 0.626 | 0.0003 | 1.409 | 1.604 |

For the investigation of differences between the traditional and the proposed methods, and for the clarification of the influences of additional perturbing forces we provide simulations for various apparent velocities and altitudes of entry.. In these simulations, we varied the value

of apparent velocity in diapason from 12 km/s to a maximum value corresponding to the elliptical motion. For all these simulated meteoroids the same altitude of entry point at 70 km was used. In addition, these meteors have different values of elevations. Initial conditions for modelling presented in table 4.

Table 4. Initial conditions for numerical simulation.

| # | $t_0$ | $\varphi$, ° | $\lambda$, ° | $h_e$, km | Az, deg | El, deg | $V_e$, km/s |
|---|---|---|---|---|---|---|---|
| 1 | 2010-02-28 22:24:47.0 | 48.467 | 20.705 | 70.0 | 252.66 | 60.20 | 12…18 |
| 2 | 2013-09-13 22:33:47.0 | 61.458 | 26.900 | 70.0 | 238.94 | 55.06 | 12…16.5 |
| 3 | 2010-12-26 14:06:09.0 | 64.780 | 26.910 | 70.0 | 156.20 | 25.80 | 12…31 |
| 4 | 2014-09-25 03:12:15.0 | 66.520 | 25.160 | 70.0 | 357.25 | 11.05 | 12…19 |

The results of numerical simulations (presented in appendix 4) illustrate the differences between the traditional and the proposed approach. Additionally, the estimated influences of the perturbing forces on the orbital elements are presented in appendix 5. For a comparison of between the two methods, a model of the Earth as a point mass was used. To estimate the influences of additional perturbing forces, we took into account Earth's flattening and the Moon's gravitational attraction.

We then interpreted the differences seen in the results of the two methods and the two perturbation sets as well, to get an estimate of the accuracy of each method and each force model.

As we can see in appendix 4, when examining the semi-major axis the greatest difference between the two methods are recorded in the high velocity cases The differences are much less significant for low velocity particles. The largest values of differences are 0.08 a.u. and 0.10 a.u. for model particle #1 and #4, respectively. The influences from the perturbing follow a similar behavior, but the value of its impact is much less: for particles #3 and #2, their values are 0.035 a.u. and 0.020 a.u., respectively.

For the eccentricity, and other orbital elements we can see a directly opposite trend: the greatest differences corresponds to the low velocity cases: 0.012 for particle #1 and 0.005 for particles #2 and #4. A similar behavior takes place on the orbit's eccentricity caused by the perturbations of the Moon and by Earth flattening. The values increase to 0.0008 and 0.0006 for particles #4 and #3.

In the case of orbit inclination, the differences between the two methods and the two sets of perturbations also demonstrate a similar behavior: the values increased for low-velocity meteoroids. In the simulations of the two different methods, this effect achieves a value of about 0.27 degrees for particle #2. For the simulations observing the two sets of perturbations, the most

significant difference occurs in the case of test particle #4 where the value reached 0.020 degrees.

For longitude of ascending node the two methods, have a difference of more than 0.4 degrees while the two sets of perturbation have a difference of - 0.015 degrees. These values are much higher than the initial values accuracy by which this parameter can be obtained. For the argument of periapsis the differences between two methods exceed 3 and 1.25 degrees for particle #1 and for particles #2 and #4, respectively. The differences between the two sets of perturbation in this case reach 0.05 and 0.03 degrees for particle #1 and for particles #2.

Therefore, taking into account high precision of calculation of longitude of ascending node $\Omega$, the numerical integration of equation of motion is recommended in place of those suing the introduction of corrections for zenith attraction. The inclusion of additional perturbing forces to the analysis is recommended for cases involving low velocity meteoroids.

**Conclusions**

We have implemented a technique to determine a meteor's orbit that is based on the numerical integration of differential equations of motion. The technique also takes into account the perturbations due to Earth's gravitational field (both the spherical part and the non-central part of the geopotential), perturbations from the atmospheric drag, perturbations from the Moon, and from other planets of the solar system. The obtained results show good correspondence with various implementations of the traditional technique, which are based on zenith attraction factors.

The analysis of the contributions of various sources of perturbation on the resulting meteoroid orbit shows that the orbits obtained by our method, are generally consistent with the results obtained by the traditional zenith attraction approach. The differences between the results obtained by the two methods increase with a decrease in pre-atmospheric velocity value and/or the lowering of the initial height of a meteor.

Based on our investigations, the attraction of the Moon and the effect of Earth flattening are seen as the main factors perturbing a meteoroid's orbit, second only to that of the Earth as a point mass. These perturbations are generally expressed in the orbital elements of the argument of the periapsis and the mean anomaly of the meteoroid (see Table 3).

Our methods are incorporated in software called Meteor Toolkit which can be used to integrate the equations of motion back in time, preceding an impact, as well as forward in time to the moment of impact with the Earth’s surface. It can be used both for meteoroids and near Earth asteroids. Meteor Toolkit is freely available from the authors upon request.

**Acknowledgments**

Meteor Toolkit uses freely distributed procedures and kernels of SPICE system (Acton, 1996) and the authors are grateful to its developers. This work was carried out at MIIGAiK and supported by the Russian Science Foundation, project No. 14-22-00197. We are very grateful to Esko Lyytinen for his excellent help with selection of the fireballs recorded by the Finnish Fireball Network and preliminary data analysis. We also thank other members of the Finnish Fireball Network who made application of the model to real cases possible through their observational efforts. In particular, we would like to thank Jarmo Moilanen, Asko Aikkila, Aki Taavitsainen, Jani Lauanne, Pekka Kokko, and Panu Lahtinen. Matti Tarvainen (Institute of Seismology, Department of Geosciences and Geography, University of Helsinki, Finland) and Peter Völger (Swedish Institute for Space Physics (IRF), Kiruna, Sweden) are kindly acknowledged for providing the seismic and atmospheric data used in fireball data analysis. We are grateful to Prof. José María Madiedo and anonymous reviewer for their comments and suggestions which significantly improved and expanded the previous version of this paper. The authors thank Prof. Jürgen Oberst for group meetings and a number of constructive discussions on this topic at MIIGAiK, and his preliminary review of this study. The authors are grateful to Jeffrey Brower (RASC) for his help with language correction.

## References


Acton, C. (1996). Ancillary Data Services of NASA's Navigation and Ancillary Information Facility. *44*(1), pp. 65-70.

Andreev, G. (1990). The Influence of the Meteor Position on the Zenith Attraction , International Meteor Organization. In D. Heinlein, & D. Koschny (Ed.), *Proceedings of the International Meteor Conference*, (pp. 25-27). Violau, Germany, 6-9 September 1990.

Bettonvil, E. (2006). Software for Orbit Determination at the KNVWS Meteor Section, Proceedings of the First Europlanet Workshop on Meteor Orbit Determination. In J. McAuliffe, & D. Koschny (Ed.), *Proceedings of the First Europlanet Workshop on Meteor Orbit Determination*, (pp. 37-41). Roden, The Netherlands, 11-13 September 2006.

Borovicka J., et al. (2013). The Kosice meteorite fall: Atmospheric trajectory, fragmentation, and orbit. *Meteoritics & Planetary Science, 48*(10), pp. 1757–1779.

Bouquet A., et al. (2014). Simulation of the capabilities of an orbiter for monitoring the entry of interplanetary matter into the terrestrial atmosphere. *Planetary and Space Science, 103*. pp. 238–249

Brown P., et al. (2011, March). he fall of the Grimsby meteorite: Fireball dynamics and orbit from radar, video, and infrasound records. *Meteoritics & Planetary Science, 46*(3), pp. 339–363.

Ceplecha, Z. (1987, July). Geometric, dynamic, orbital and photometric data on meteoroids from photographic fireball networks. *Astronomical Institutes of Czechoslovakia, Bulletin (ISSN 0004-6248)*, pp. 222-234.

Chambers, J. E. (1999). A hybrid symplectic integrator that permits close encounters between massive bodies. *Monthly Notices of the Royal Astronomical Society, 304*(4), pp. 793-799.

Clark, D. L., & Wiegert, P. A. (2011, Aug). A numerical comparison with the Ceplecha analytical meteoroid orbit determination method. *Meteoritics & Planetary Science, 46*(8), pp. 1217–1225.

de la Fuente Marcos, C., & de la Fuente Marcos, R. (2013). The Chelyabinsk superbolide: a fragment of asteroid 2011 EO40? *Monthly Notices of the Royal Astronomical Society Letters, 436*(1), pp. L15-L19.

Folkner, W., Williams, J., & Boggs, D. ( 2009, August 15 ). The Planetary and Lunar Ephemeris DE 421. *IPN Progress Report 42-178*, p. 34.

Gritsevich, M. (2010). On a Formulation of Meteor Physics Problems. *Moscow University Mechanics Bulletin,, 65*(4), pp. 94-95.

Gritsevich, M., Lyytinen, E., Moilanen, J., Kohout, T., Dmitriev, V., Lupovka, V., et al. (2014b). First meteorite recovery based on observations by the Finnish Fireball Network. In J. Rault, & P. Roggemans (Ed.), *Proceedings of the International Meteor Conference 2014*, (pp. 162-169). Giron, France.

Gritsevich, M., Vinnikov, V., Kohout, T., Toth, J., Peltoniemi, J., Turchak, L., et al. (2014a). A comprehensive study of distribution laws for the fragments of Kosice meteorite. *Meteoritics & Planetary Science, 49*(3), pp. 328-345.

Gural, P. S. (2001). Fully Correcting for the Spread in Meteor Radiant Positions Due to Gravitational Attraction. *WGN, Journal of the International Meteor Organization*, pp. 134-138.

Jenniskens P. et al. (2012). Radar-Enabled Recovery of the Sutter's Mill Meteorite, a Carbonaceous Chondrite Regolith Breccia. *Science, 338*(6114), pp. 1583-1587.

Kohout et al. (2014). Density, porosity and magnetic susceptibility of the Kosice meteorite shower and homogeneity of its parent meteoroid. *Planetary and Space Science, 93*, 96-100.

Langbroek, M. (2004). A spreadsheet that calculates meteor orbits. *Journal of the International Meteor Organization, 32*(4), pp. 109- 110.

Lyytinen, E., & and Gritsevich, M. (2013). A flexible fireball entry track calculation program. In Proceedings of the International Meteor Conference 2012. In M. Gyssens, & P. Roggemans (Ed.), *Proceedings of the International Meteor Conference*, *2*, pp. 155–167. La Palma, Spain, 20-23 September 2012.

Lyytinen, E., & Gritsevich, M. (2015). Implications of the atmospheric density profile in processing of the fireball observations. *Planetary and Space Science, submitted*.

Madiedo, J. M., Trigo-Rodríguez, J. M., Ortiz, J. L., Castro-Tirado, A. J., & Cabrera-Caño, J. (2014). Bright fireballs associated with the potentially hazardous asteroid 2007LQ19. *Monthly Notices of the Royal Astronomical Society, 443(2)*, 1643-1650.

Madiedo, J. M., Trigo-Rodríguez, J. M., Williams, I. P., Ortiz, J. L., & Cabrera, J. (2013). The Northern χ-Orionid meteoroid stream and possible association with the potentially hazardous asteroid 2008XM1. *Monthly Notices of the Royal Astronomical Society, 431(3)*, 2464-2470.

Milley, E. P. (2010). Physical Properties of Fireball-Producing Earth-Impacting Meteoroids and Orbit Determination through Shadow Calibration of the Buzzard Coulee Meteorite Fall. *ProQuest Dissertations And Theses; Thesis (M.Sc.)*. University of Calgary.

Montenbruck, O., & Gill, E. (2000). *Satellite Orbits, Models, Methods and Applications.* Springer-Verlag.

Petit, G., & Luzum, B. (Eds.). (2010). IERS Conventions. p. 179. Frankfurt am Main: Verlag des Bundesamts fur Kartographie und Geodasie.

Picone, J., et al. (2002). NRLMSISE-00 empirical model of the atmosphere: Statistical comparisons and scientific issues. *Journal of Geophysical Research: Space Physics, 107*(A12), p. 1468.

Plakhov, Y., et al. (1989). Method for the numerical integration of equations of perturbed satellite motion in problems of space geodesy. *Geodeziia i Aerofotos'emka, 4*, pp. 61-67.

Popova, O.P., Jenniskens, P. et al. (2013). Chelyabinsk Airburst, Damage Assessment, Meteorite Recovery, and Characterization. *Science, 342* (6162 ), pp. 1069-1073.

Rice, J. (2006). *Mathematical Statistics and Data Analysis.* Belmont, California: Cengage Learning.

Spurny, P., Oberst, J., & Heinlein, D. (2003, May). Photographic observations of Neuschwanstein, a second meteorite from the orbit of the Pribram chondrite. *Nature, 423*(6936), pp. 151–153.

Standard Atmosphere, 1976. (1976). *States Committee on Extension to the Standard Atmosphere (COESA)*. US Government Printing Office, Washington, DC.

Standards of Fundamental Astronomy Board. (2013, October 31). *Release 10*. International Astronomical Union Division A: Fundamental Astronomy.

Trigo-Rodriguez, J., Lyytinen, E., Gritsevich, M., Moreno-Ibanez, M., Bottke, W., Williams, I., et al. (2015). Orbit and dynamic origin of the recently recovered Annama's H5 chondrite. *Monthly Notices of the Royal Astronomical Society,* 449(2), pp. 2119-2127.

Vaubaillon, J. et al. (2015). The 2011 Draconids: the first European airborne meteor observation campaign. *Earth, Moon, and Planets, 114*(3-4), pp. 137-157.

Zoladek, P. ( 2011). PyFN –multipurpose meteor software. In M. Gyssens, & P. and Roggemans (Ed.), *Proceedings of the International Meteor Conference*, (pp. 53-55). Sibiu, Romania, 15-18 September, 2011.

Zuluaga, J. I., Ferrin, I., & Geens, S. (2013). The orbit of the Chelyabinsk event impactor as reconstructed from amateur and public footage. *Earth and Planetary Science Letters arXiv:1303.1796*.

**Appendix 1.** Explanation of the symbols used in Table 1 and 3.

Topocentric radiant:

| | |
|---|---|
| $B$ | = the geodetic latitude of the initial point of the fireball |
| $L$ | = the geodetic longitude of the initial point of the fireball |
| $A$ | = the apparent azimuth of the fireball track at its initial point (from the north) |
| $El$ | = the apparent elevation of a fireball's track at its initial point |
| $V$ | = the apparent geocentric velocity of the fireball at its initial point |

Orbital elements:

| | |
|---|---|
| $a$ | = the semimajor axis |
| $e$ | = the eccentricity |
| $i$ | = the inclination |
| $\Omega$ | = the longitude of the ascending node |
| $\omega$ | = the argument of periapsis |
| $M$ | = the mean anomaly at epoch |

**Appendix 2.** Minimum Windows System Requirements for Meteor Toolkit.

Meteor Toolkit is an executable file along with some additional dependent libraries. Also note, although Meteor Toolkit uses SPICE libraries and subroutines, they do not need to be compiled as they are assembled into a portable dll.

The minimum system requirements are:

| | |
|---|---|
| Operating system | Windows (XP, Vista, 7, 8) x86 and x64 architecture. .NET Framework not lower than 3.5. |
| CPU | 0.8GHz (Windows XP) |
| Memory | 512 MB RAM (Windows XP) |
| Hard drive | 30 MB free space on disk |

**Appendix 3.** “Meteor Toolkit”: GUI of Meteor Toolkit, software for determining a meteor's orbit.

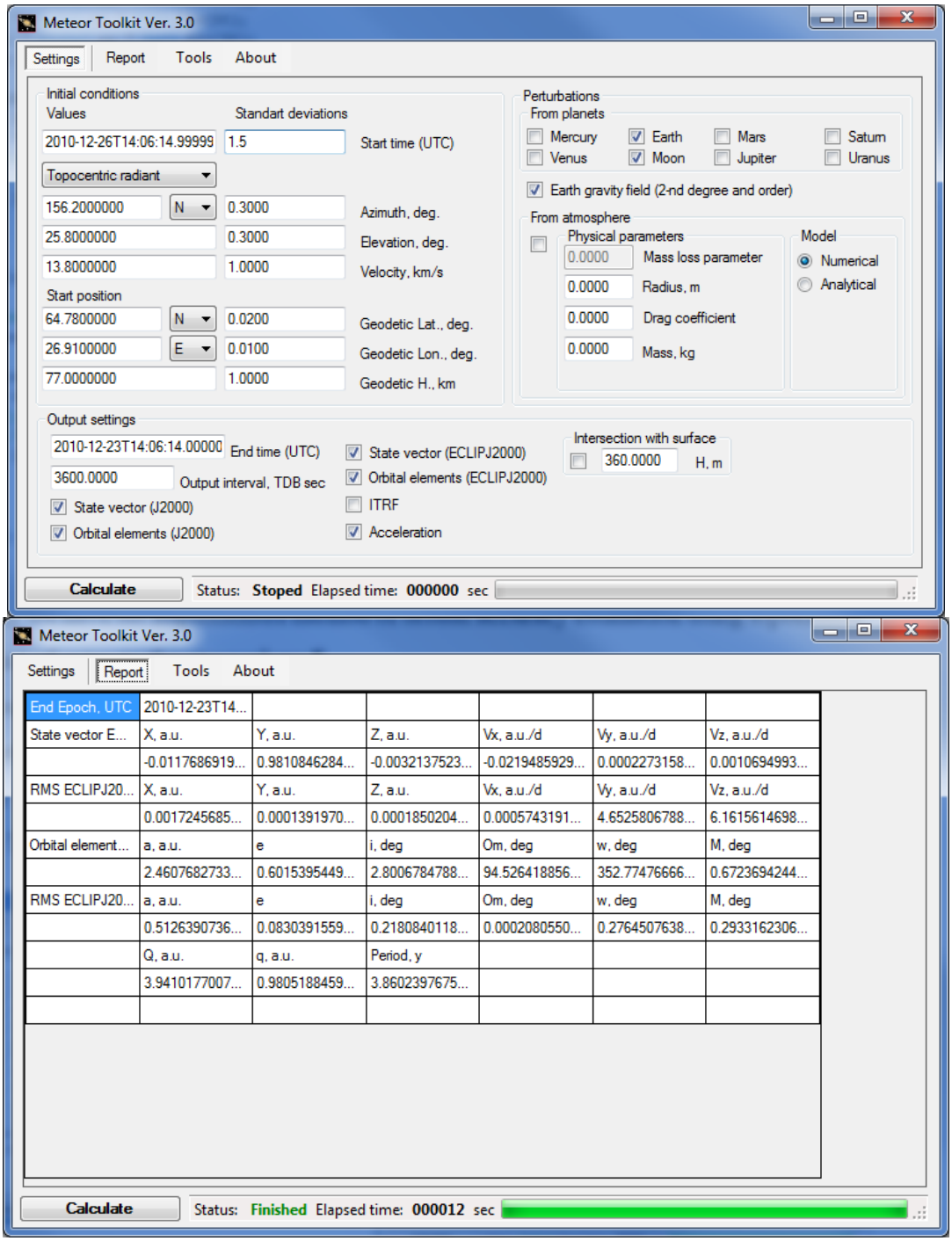

**Appendix4**. Differences between orbits of simulated meteoroids calculated using traditional approach and proposed technique. Initial data are presented in appendix 4. Perturbations from attraction due Earth's flattening and Moon was taking into account.

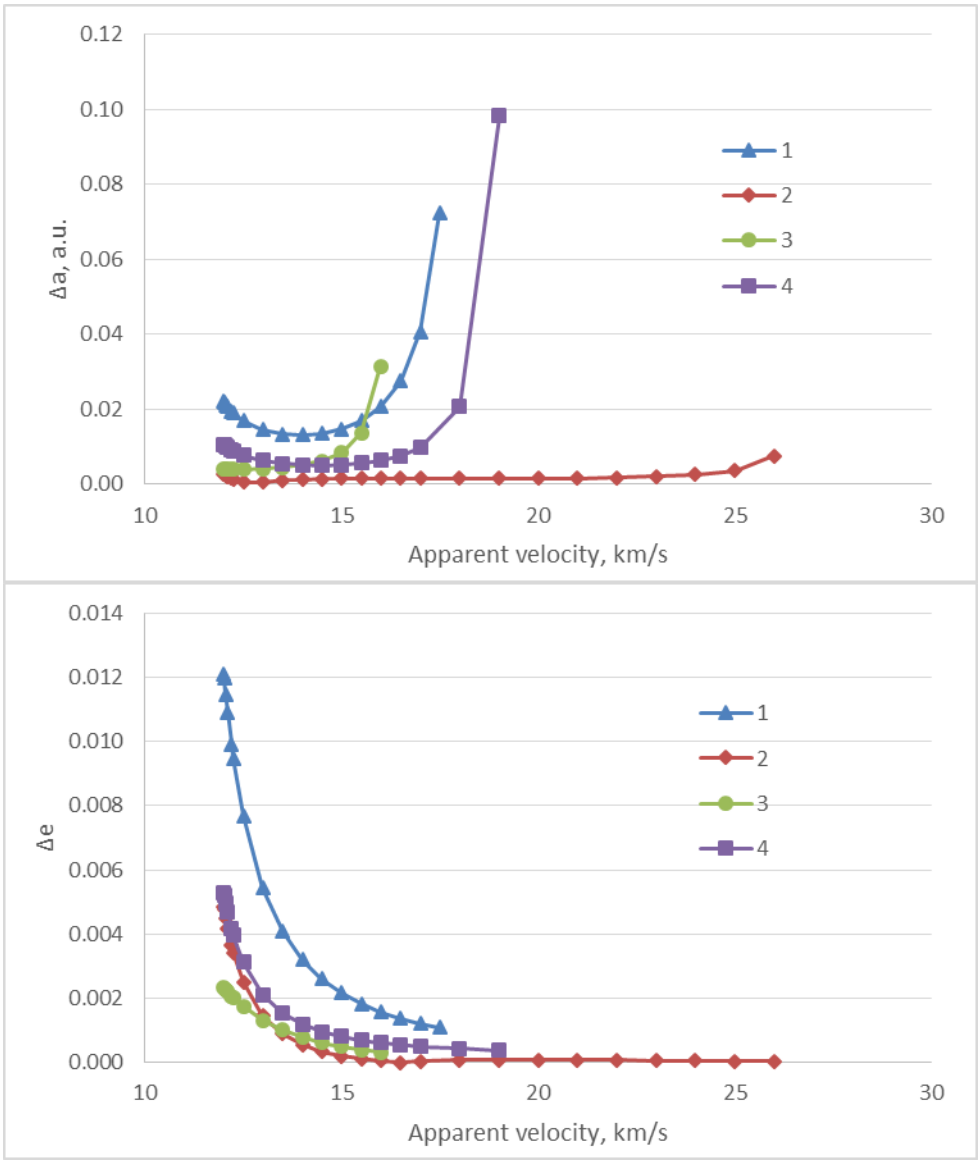

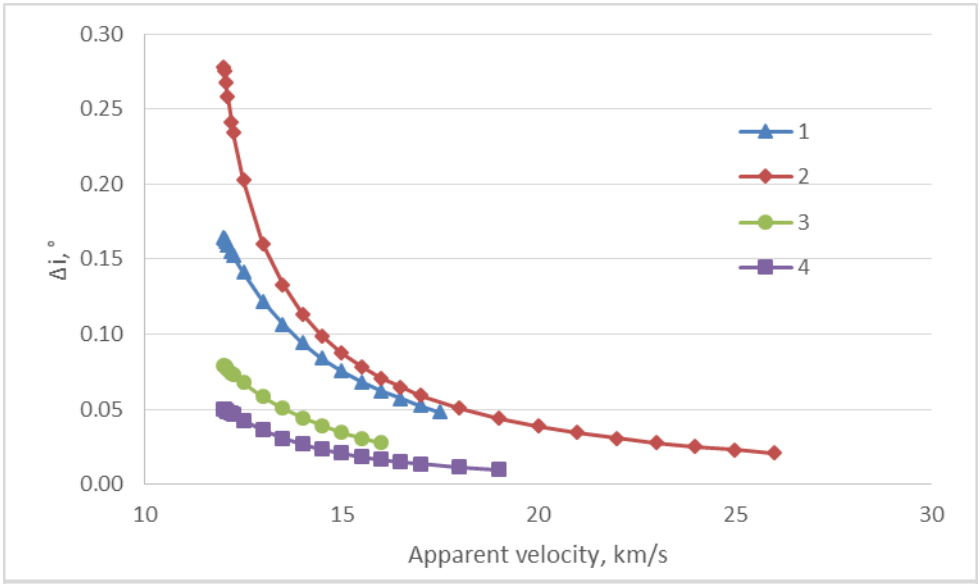
0.30
0.25
0.20
0.15
0.10
0.05
0.00
Δi, °
10
15
20
25
30
Apparent velocity, km/s
1
2
3
4

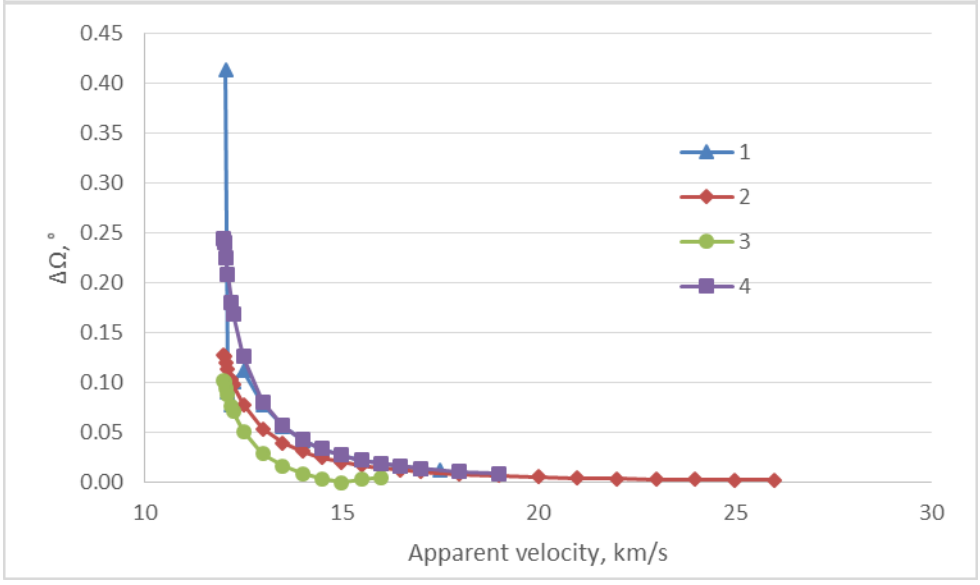
0.45
0.40
0.35
0.30
0.25
0.20
0.15
0.10
0.05
0.00
ΔΩ, °
10
15
20
25
30
Apparent velocity, km/s
1
2
3
4

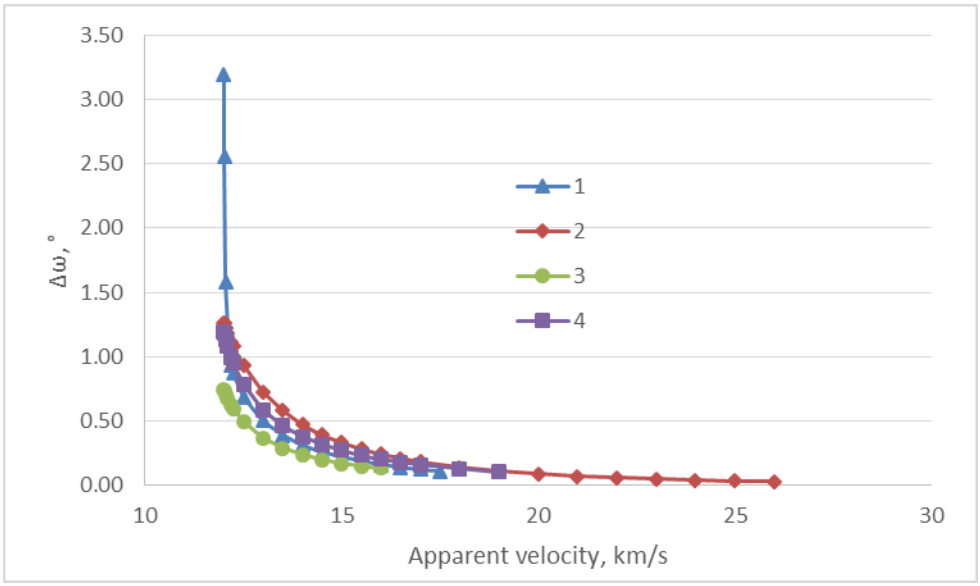
3.50
3.00
2.50
2.00
1.50
1.00
0.50
0.00
Δω, °
10
15
20
25
30
Apparent velocity, km/s
1
2
3
4

**Appendix 5.** Differences between orbits of simulated meteoroids calculated with proposed technique by using Earth attraction as point mass and by using perturbation from Earth's flattening and Moon as well.

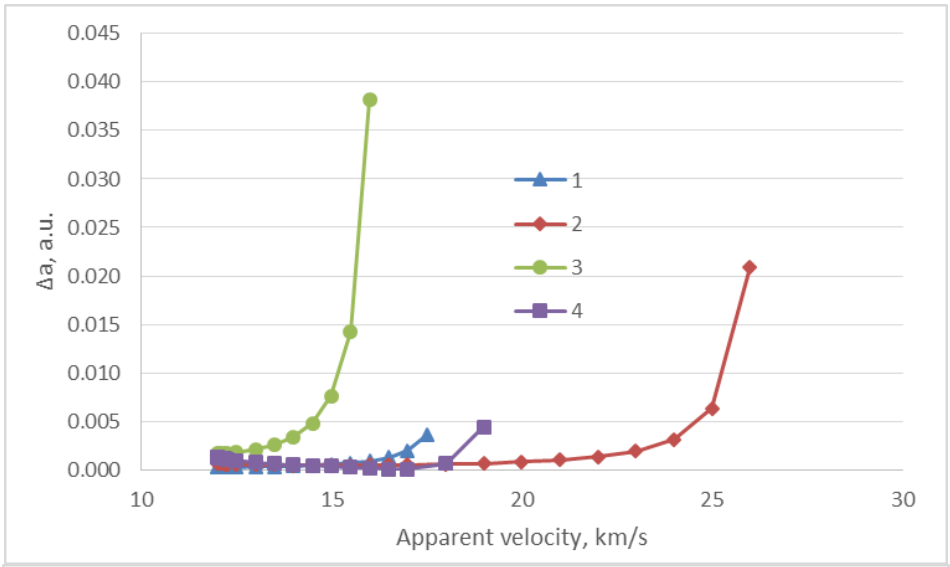


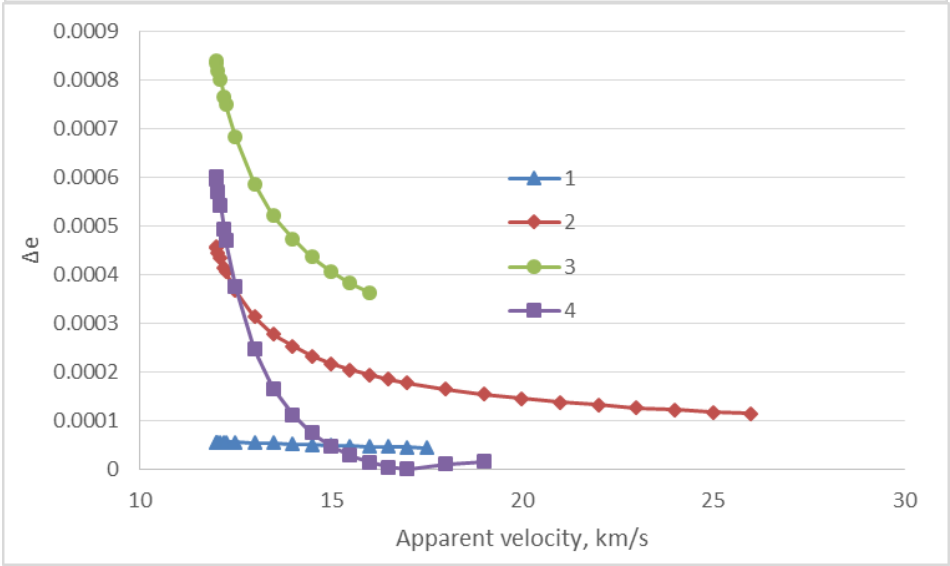


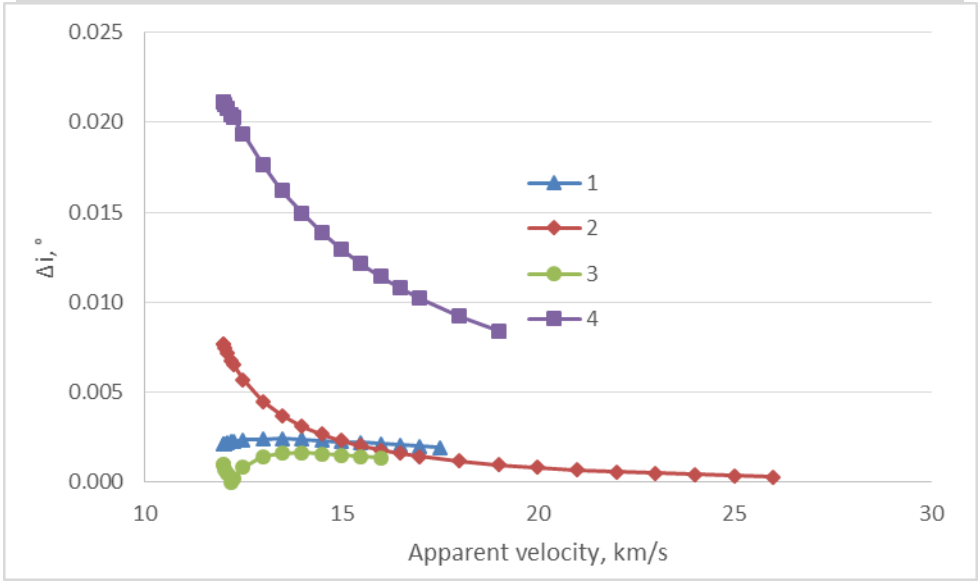

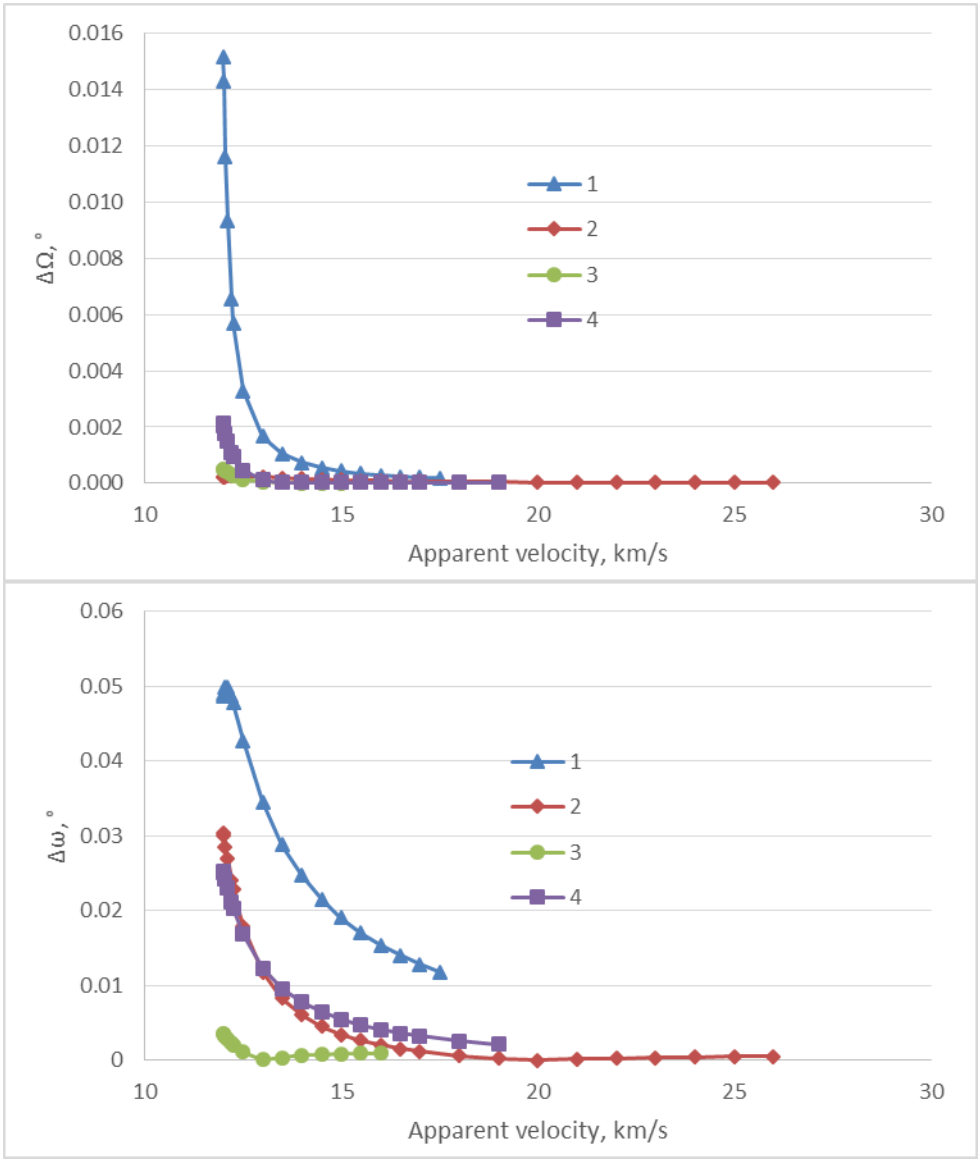
0.016
0.014
0.012
0.010
0.008
0.006
0.004
0.002
0.000
ΔΩ, °
1
2
3
4
10
15
20
25
30
Apparent velocity, km/s
0.06
0.05
0.04
0.03
0.02
0.01
0
Δω, °
1
2
3
4
10
15
20
25
30
Apparent velocity, km/s